JOURNAL OF PROPULSION AND POWER
Vol. 14, No. 1, January–February 1998

Characteristics of a Trapped-Vortex Combustor

K.-Y. Hsu* and L. P. Goss†
Innovative Scientific Solutions, Inc., Dayton, Ohio 45440-3638
and
W. M. Roquemore‡
U.S. Air Force Wright Laboratory, Wright–Patterson Air Force Base, Ohio 45433-7103

Combustion characteristics are described for a conceptual combustor that utilizes a trapped vortex (TV) in a cavity to provide flame stability. The cavity is formed between two axisymmetric disks mounted in tandem. The upstream disk is referred to as the forebody, and the downstream disk is referred to as the afterbody. With coflowing annular air, a vortex is trapped in the cavity for certain geometries. Primary air and gaseous propane are injected directly into the cavity through multiple jets located on the upstream face of the afterbody. Particle-imaging-velocimetry measurements reveal that when the cavity length is 0.59 of the forebody diameter, a vortex is trapped in the cavity. Very low overall lean-blow-out equivalence ratios are obtained for the TV combustor over a wide range of annular- and primary-airflow rates. Temperature profiles obtained with a coherent-anti-Stokes-Raman-spectroscopy system show that as the primary-airflow rate increases (equivalence ratio approaches unity), the temperature in the vortex increases for a fixed fuel flow. An increase in the primary-airflow rate also results in a decrease in the flame length. Peak combustion efficiency increases from 96.7 and 99% as the annular air is decreased, and to 98.8 and 99.8% when a second trapped vortex is added to the combustor via a second afterbody just downstream of the first afterbody.

Introduction

COMBUSTION stability is often achieved using recirculation zones to provide continuous sources of ignition by mixing hot products and burning gases with the incoming fuel and air. Swirl vanes, bluff-bodies, and rearward-facing steps are commonly used methods of establishing recirculation zones for flame stabilization. This paper investigates the use of cavities as a means of stabilizing flames. In 1957, Huellmantel et al.[1] investigated recesses in a wall as a means of improving flame stability and reducing the pressure drop across a combustor. They evaluated 12 recess or cavity configurations in a small 2.5 cm by 4.5 cm tunnel and found the blow-out velocities of premixed propane/air flames to be considerably higher for recessed flameholders and to have lower pressure drops than a V-gutter flameholder. They also found that flame stability was not sensitive to the shape of the recess as long as separation was present at the leading edge of the recess. Morrison et al.[2] investigated the blowout limit of a cavity with fuel injected directly into the recirculation zone. Although their results did not fully characterize the performance of the cavity, they did support the idea that cavity flameholders could result in a compact ramjet/scramjet combustor design. Niioka et al.[3] investigated the flame-stabilization characteristics of a cavity between two struts. Hydrogen fuel was injected along the centerline of the cavity. They found that flame stability could be achieved in a flow with a freestream Mach number of 1.5, but that the stability was strongly dependent on the separation of the two struts. Willis et al.[4] investigated the use of a dump-cavity combustor as a means of waste destruction. The waste was injected directly into the cavity. The waste was completely destroyed when the combustor operated in a quiet mode in which the recirculation zone in the cavity was stable. They identified the cavity lengths and premixed fuel-to-air ratios that yielded stable and unstable combustion.

Cavities have been extensively investigated by the aerodynamic community as a means of recovering pressure or reducing drag. Indeed, the term trapped vortex was applied to devices discussed by Ringleb[5] for controlling flow separation as applied to diffusers. The rules for sizing cavities to reduce the drag of bluff-bodies was investigated by Mair[6] and Little and Whipkey,[7] who investigated cavities formed between two axisymmetric disks spaced along a central spindle. Mair[6] showed that for the ratio of afterbody-to-forebody disk diameters of <1, an optimal separation distance existed where the drag was a minimum. Furthermore, the minimum drag was considerably lower than that of the forebody disk alone. Mair[6] also found that for a given afterbody diameter, there were separation distances where the drag increased dramatically above that of the forebody alone. Little and Whipkey[7] showed that the minimum drag corresponds to the condition where the recirculation zone is stable. They established a correlation between the disk separation distance and afterbody disk diameter, both being normalized by the forebody disk diameter, which yielded a stable or locked vortex. Gharib and Roshko[8] reviewed other studies in which low- and high-drag conditions were achieved by changing the cavity size. They also performed a systematic investigation of the process and concluded that low drag occurs when the cavity shear layer stagnates at the downstream corner of the cavity. When this happens, the vortex motion in the cavity is stable.[7] Gharib and Roshko[8] associated the low-drag condition with self-sustained cavity flow oscillations through a feedback mechanism that maintains the locked-on position of the stagnation zone to the downstream corner of the cavity. Thus, the feedback mechanism helps maintain a stable vortex in the cavity, even when external fluid is injected directly into the cavity.[9] Katta and Roquemore[10] used a time-dependent, axisymmetric mathematical model to predict the results of Mair[6] and Little and Whipkey,[7] and the combusting results of Hsu et al.[11] The simulations showed that a vortex

Presented as Paper 95-0810 at the AIAA 33rd Aerospace Sciences Meeting, Reno, NV, Jan. 9–12, 1995; received July 5, 1996; revision received Aug. 20, 1997; accepted for publication Aug. 29, 1997.

*Senior Engineer, 2786 Indian Ripple Road. Member AIAA.
†President and Director of Research, 2786 Indian Ripple Road. Member AIAA.
‡Senior Scientist, Aero Propulsion and Power Directorate, Fuels and Lubrication Division. Member AIAA.

was trapped in the cavity when the afterbody diameter and disk separation were consistent with the rules established by Little and Whipkey.[7] The simulations also showed that a vortex would be trapped in the cavity when the stagnation point was located at the downstream corner of the cavity.[8] Furthermore, when a vortex was trapped in the cavity, very little fluid was entrained into the cavity. The cavity entrainment was estimated using lean-blow-out (LBO) data under various cavity lengths and flow conditions by Sturgess and Hsu.[12]

To our knowledge, the flame-stability characteristics of cavities that are aerodynamically designed to trap a vortex have not been investigated. One reason for this may be that when a vortex is trapped in a cavity, very little exchange of main flow and cavity fluid occurs. This constitutes a problem because flame stability requires a continuous exchange of mass and heat between the cavity and main flow. This problem can be solved by directly injecting both fuel and air into the cavity in a manner that reinforces the vortex. The goal of the present study was to investigate the flame-stability characteristics of a trapped vortex (TV) combustor in which fuel and air are injected directly into the cavity from the face of the afterbody. This back-face fuel-injection scheme is similar in appearance to the T and mushroom vaporizers used in prevaporizing combustion chambers.[13] However, in vaporizer combustion systems, the flame is not stabilized by a vortex trapped in a cavity. In a TV combustor, the flame in the cavity is not directly exposed to the high inlet velocities of a main airflow; therefore, a TV combustor has the potential of providing stable operation over a wide range of inlet airflow rates and fuel-to-air ratios while maintaining high combustion efficiencies, low lean-blow-out-limits, and a low-pressure drop. Low nitric oxide (NO_x) emissions might also be achievable by controlling fuel-to-air ratio, mixing, and residence time in a cavity pilot burner and a main burner. As noted in the studies of Huellmantel et al.,[1] wall heating and the influence of cooling air on the combustion process are concerns with this method of flame stabilization. This paper describes preliminary investigations of the influence of cavity size on the pressure drop across the combustor and on the LBO limits. Combustion efficiency and emissions are also investigated as a function of fuel-to-air ratio in the cavity and inlet–air velocity.

Experimental Descriptions

The combustor used in this study consists of a forebody and an afterbody (Fig. 1a). Stainless steel was used in fabricating the combustor assembly. The afterbody is connected to two concentric tubes along the centerline of the forebody. Fuel and primary air are delivered through these concentric tubes to two separate chambers in the afterbody that is 50.8 mm in diameter. The forebody, having a diameter d_f of 70 mm, is located at the exit plane of the vertically mounted annular-air duct that has a diameter of 80 mm. The blockage ratio, defined as the ratio of the area of the forebody to that of the air duct, is 76%. A maximum averaged annular-air velocity of 42 m/s can be achieved with this configuration. An axisymmetric cavity, defined as the void region between the forebody and the afterbody, is used. The cavity length H is defined as the axial distance between the forebody and afterbody, as noted in Fig. 1a. The cavity length is adjustable and is an important parameter in this study. The unheated annular- and primary-air flows originate from two air supplies that are controlled and metered separately. The experiment was conducted under atmospheric conditions.

The arrangement of fuel and primary-air injection on the afterbody is shown in Fig. 1b. Gaseous-propane fuel is injected through eight orifices (1.75 mm in diameter), and the primary air is supplied through 24 orifices (2.29 mm in diameter) surrounding the fuel jets. The fuel and primary air are injected near the centerline to follow the natural recirculation flow pattern created in the cavity. Direct injection of primary air serves several purposes: 1) it provides direct control of the local equivalence ratio inside the recirculation zone, 2) it enhances mixing by increasing the mixing region through distributed fuel and air jets, and 3) it provides some cooling for the injector assembly. A water manometer is used to measure the static pressure drop across the combustor over a range of cavity-length and inlet-flow conditions. The LBO limits of this combustor were tested over a range of primary- and annular-airflow conditions.

A 35-mm camera and a video recorder were used to record the flame images under various flow conditions. The instantaneous velocity field was obtained using the two-color particle-imaging-velocimetry (PIV) technique.[14,15] A pulsed Nd:YAG laser and a Nd:YAG-pumped dye laser were used for generating two different wavelengths to eliminate ambiguity in determining the flow direction. Cylindrical lenses were employed to form a laser sheet vertically across the centerline of the burner. Monospherical particles of Al_2O_3 (5 μm in diameter) were seeded through the primary airjets. A 35-mm camera mounted at a right angle to the laser sheet was used to record the images of the particles illuminated by the laser. A synchronization circuit was employed to control the time separation between the two laser pulses. The typical time separation was set to ~30 μs for the flow conditions studied. A color scanner was used to digitize the images, and the data were stored in a computer for further analysis. The data analysis and experimental setup of the two-color PIV technique are treated in detail in Refs. 14 and 15.

The radial temperature was profiled at different axial locations inside the recirculation zone using the coherent-anti-Stokes-Raman-spectroscopy (CARS) technique. The CARS system employed in this study was based on a Nd:YAG/broadband dye–laser combination tuned for N_2 excitation. An intensified charge-coupled device (CCD) camera mounted at the exit plane of the monochromator was interfaced with a com-

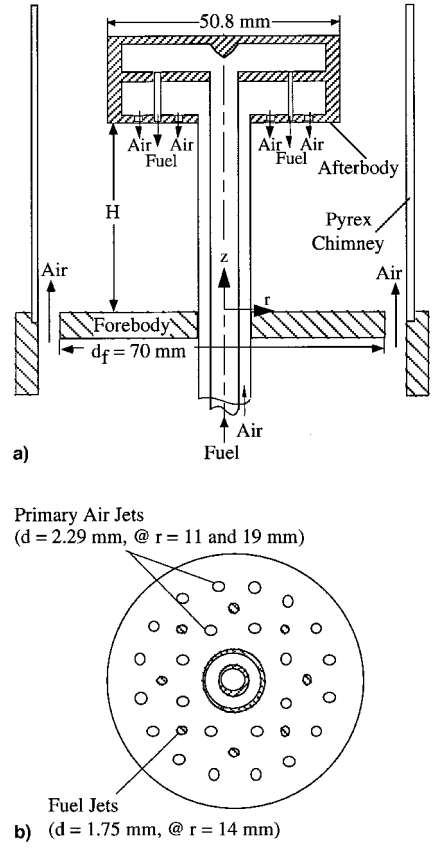

Fig. 1 Schematic diagrams of a) trapped-vortex combustor and b) injection plane of afterbody.

puter for single-shot broadband spectrum detection. Temperature information was obtained using a nonlinear least-squares routine to fit the measured spectra. The shot-to-shot and mean errors of the temperature measurements resulting from this CARS system were estimated to be about 5 and 1%, respectively. At each spatial location, 1000 spectra were collected at a rate of 10 Hz, and the mean and rms temperatures at each spatial location were plotted.

Emission measurements were made under various flow conditions to further characterize the performance of the combustor. A portable emission-sampling/analyzer unit was used to measure the concentrations of CO, NO_x, O_2, and unburned hydrocarbon (UHC) at the exit of the combustor. The equilibrium CO_2 concentration was calculated from the measured O_2 concentration. A routine was then used to calculate the exhaust equivalence ratio and combustion efficiency based on the gas sample collected. The flow was confined by a Pyrex® tube (80 mm i.d.), 910 mm in length, to eliminate the uncertainty in the measurement resulting from entrained ambient air. The gas samples were collected at an axial location z = 860 mm downstream from the face of the forebody. The preliminary single-point measurements were made using stainless-steel tubing (3-mm i.d.) as the sampling probe. The radial profiles of emission concentration were generally uniform, except under certain flow conditions. For obtaining the overall emission characteristics of the combustor for comparison purposes, a probe with multiple holes was used to measure the averaged emission concentrations. The probe was placed inside the glass chimney and intersected the centerline of the flow. Five holes (0.4 mm in diameter), located at the same axial location, were placed at specific radial locations to collect area-weighted samples. The uncertainty between the measured equivalence ratios and the metered overall equivalence ratios was found to be within 10% under the flow conditions studied. The analyzer was calibrated with calibration gases; however, the absolute values of the concentrations may be biased because of the noncooled sampling probe. Because only the trends of the emission characteristics of the combustor were of interest in this study, the quenching of reactions from the sampling were not investigated. During the emission measurements, flame lengths were also measured visually under various flow conditions.

Results

Preliminary experiments were conducted to determine the impact of afterbody diameter and cavity length on the flame structure. The diameter of the forebody was fixed at 70 mm for this study. Three afterbodies having different diameters were investigated, and the cavity length for each was systematically varied under combusting conditions. Although this was a preliminary investigation, it did show that the visual flame structure is strongly dependent on afterbody diameter and cavity length. An afterbody having a diameter of $0.73d_f$ was used because it was observed to produce the most stable flame. The results will be presented in the following sequence: 1) choice of optimal cavity length based on the criteria of low-pressure drop and low LBO limits; 2) impact of primary air on LBO, velocity and temperature fields, emissions and combustion efficiency, and flame length; and 3) impact of adding a second afterbody on emissions and combustion efficiency.

Cavity Length

Figure 2 shows the impact of cavity length on pressure drop across the combustor for different annular-air flows under nonreacting flow conditions. The primary air was turned off for this test, and the flow was confined by an 80-mm-diam, 150-mm-long Pyrex tube. The pressure drop dp is defined as the pressure difference between duct and ambient P. The normalized pressure drop dp/P for the cold flow is plotted in Fig. 2 at annular-air velocities of 14, 28, and 42 m/s. As the cavity length is varied, dp/P is observed to pass through a minimum at a cavity length of $\sim 0.6d_f$, which is more noticeable for the high annular-air flow. An increase in dp/P from 0.1 to 1.2% was measured as the annular-air velocity was increased. The results of Mair[6] and Little and Whipkey,[7] who conducted systematic studies of drag reduction for disks mounted in tandem, showed that minimum drag is achieved with an afterbody diameter of $0.75d_f$ and a cavity length of $0.6d_f$. The cold-flow data plotted in Fig. 2 are in very good agreement with their findings.

For a combusting flow at an annular air velocity U_a of 28 m/s and an overall equivalence Φ_0 of 0.12, dp/P increases to about 0.65% as compared to 0.4–0.55% for nonreacting flows. This suggests that the cavity injection and heat addition increase the pressure drop across the combustor. In the reacting flow, the pressure drop increased to around 1.5% at an annular-air velocity of 42 m/s when the combustor was operated under higher fuel loading. For combusting flow, the maximum pressure drop occurred as the cavity reached stoichiometric conditions. Although the combusting flow exhibited very little change in dp/P with cavity length at a fixed fuel flow (Fig. 2), the change in flame stability was noticeable. A stable flame with a well-defined vortex was observed visually for the cavity-length range of $0.45–0.65d_f$. Multiple vortices and vortex shedding were observed at cavity lengths $>0.65d_f$; and a quasi-steady flame existed for $<0.45d_f$. These results are consistent with the cold-flow results of Little and Whipkey,[7] who observed a stable vortex in the cavity when the cavity length corresponded to that of minimum drag. Katta[10] has studied the dynamics of the vortex structures under reacting and nonreacting flows using a time-dependent computational fluid dynamics (CFD) code. For nonreacting flows, a stable cavity flow was observed at an optimal cavity dimension that produces minimum drag. For a nonoptimal cavity dimension, vortex shedding was revealed through time-dependent calculations. The fluid injection inside the cavity also had a strong impact on the stability of the vortex in the cavity.

For achieving good combustion stability, a stable vortex in the cavity region is very desirable. The impact of cavity length on LBO limits was investigated under three annular-airflow conditions with zero primary air, and the results are shown in Fig. 3. The overall LBO equivalence ratio is <0.05 for all conditions studied. However, this ratio increases dramatically for cavity lengths $>0.65d_f$. Visual observation of the flame indicated that this increase in LBO limit is probably the result of vortex shedding at a cavity length greater than the optimum. Because the most stable flame and minimum pressure drop occurred at $0.59d_f$, this optimal cavity length was chosen for the experiments described in the following sections.

Flowfield and Flame Characteristics

Flame photographs and PIV were used to determine whether a stable vortex had formed in the TV combustor. For these experiments, the Pyrex tube was removed for optical access and, thus, the flame was unconfined. Unconfined flames are

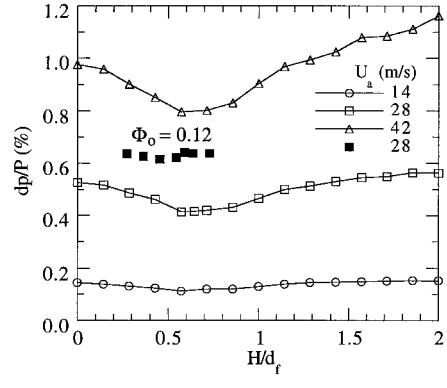

Fig. 2 Impact of cavity length H/d_f on pressure drop under cold (open) and combusting (solid) flows.

shorter and have a larger diameter near the vortex center, but have the same general features as confined flames.

The flame is visually stabilized inside the cavity; this region will be referred to as the primary zone of the combustor. The overall equivalence ratio is ~0.06 at an annular-air velocity of 28 m/s. The equivalence ratio in the primary zone Φ_p, as calculated from the fuel and primary air only, is ~1.2. The instantaneous velocity field obtained using the PIV technique is shown in Fig. 4. Repeated measurements showed that the velocity field of the large vortical structure does not change significantly from shot-to-shot, i.e., the vortex is essentially stationary. The velocity field exhibits a strong recirculating flow similar to that of a toroidal vortex. The center of the vortex is located at a radius slightly less than that of the afterbody. The radial location of the vortex center did not change significantly under different primary-air, annular-air, and fuel-flow conditions.

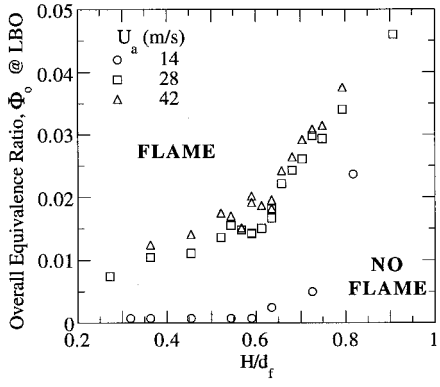

Fig. 3 Effect of cavity length H/d_f on LBO under various annular-airflows.

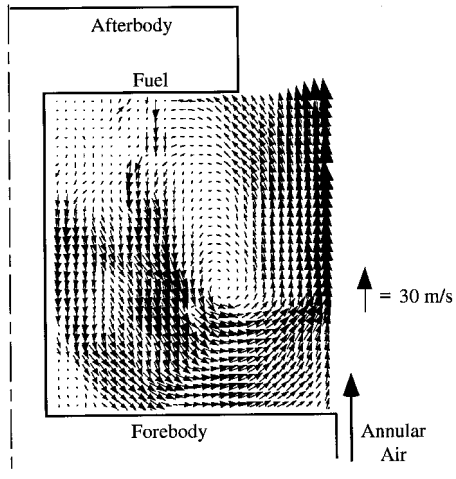

Fig. 4 Instantaneous velocity field obtained by PIV with combusting flow at U_{air} = 28 m/s.

The primary-air and fuel jets control the local equivalence ratio, mixing, residence time, and stability in the primary zone. For enhancing combustor performance, these jets should be injected in such a way that they reinforce the vortex, causing it to remain stable for a wide range of flow conditions. The velocity field in Fig. 4 includes flow from the fuel and primary-air jets, as denoted by the large velocity vectors near the afterbody face. The jets appear to dissipate before reaching the face of the forebody and be mixed into the recirculation zone and convected around the vortex center. The flow around the vortex center has a large velocity component well inside the forebody radius. Most of this fluid seems to mix with the annular air and be convected past the afterbody. However, the flow around the vortex center appears to re-enter the primary zone. The fluid contains mainly hot products and radicals that will ignite the incoming fuel and air mixtures. This process of recirculated hot products is the key to the stability of a TV combustor.

The general structure of the cavity flow appeared to be the same as that shown in Fig. 4 for a wide range of fuel and airflow conditions; this is illustrated by the flame images in Fig. 5. The annular-airflow rate was fixed at 3000 slpm and had an average velocity of 42 m/s. The fuel-flow rate was fixed at 25 slpm and had a mean fuel-jet velocity of 22 m/s. The primary air was adjusted to 56, 140, and 280 slpm, corresponding to a primary air velocity of 10, 24, and 48 m/s, respectively. The Φ_p were 11, 4.4, and 2.2, respectively, as indicated in the three flame images. The actual equivalence ratio in the cavity may be leaner because of fuel transport and additional entrainment of annular air. The overall equivalence ratio of 0.21 was not altered significantly as a result of the relatively small changes in the primary-air flows as compared with the annular-air flow. The appearance of the flame indicates that a stable vortex has formed in the cavity under these conditions. The soot concentration in the cavity region decreases with Φ_p as shown in Fig. 5. A blue flame established in the shear layer between the cavity and the annular air and anchored around the circumference of the forebody is also evident. Although the color and length of the flame varied with Φ_p, the shape of the flame in the cavity was approximately the same under all flow conditions, furnishing additional evidence that the primary zone has been stabilized by correctly sizing the cavity to trap a vortex.

The temperature fields represented by radial temperature profiles for these three conditions are shown in Fig. 6; the data were obtained with the CARS technique. Radial profiles of mean temperature are shown for axial locations of z = 5 and 40 mm, as measured from the forebody face. As the primary air increases, the axial location of the vortex center moves downstream as illustrated in Fig. 5. The third axial-temperature measurements were made intercepting the vortex center that

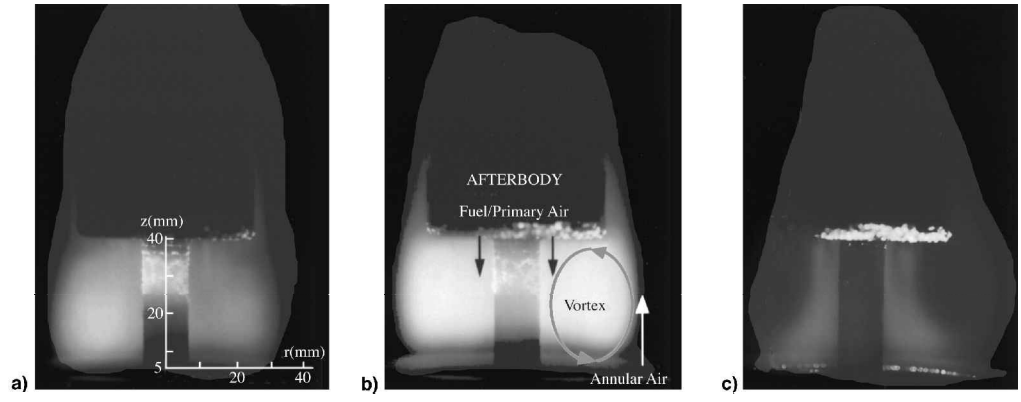

Fig. 5 Effect of primary air on flame structures at U_{air} = 42 m/s and Φ_o = 0.21. Φ_p = a) 11, b) 4.4, and c) 2.2.

changed from z = 23 to 28 mm as the primary air was increased. The unconnected symbols denote the spatial distributions of the rms of temperature.

The locations of the primary-air and fuel jets are evident in the temperature profiles in Fig. 6. The former are located at r = 11 and 19 mm, and the latter at r = 15 mm, as shown in Fig. 1b. For the weaker primary-airflow, Φ_p = 11.1, the air-jet trajectories are affected by the annular air, as evidenced by the cold-temperature zone being shifted from r = 11 to 8 mm. At higher primary-airflow rates (lower Φ_p), the stronger air jets are not disturbed by the annular air. However, the colder jet temperatures are not observed near the forebody, which suggests that the jet flows mix and react before reaching the face of the forebody.

The flame length and soot concentration decrease as the primary-airflow rate increases. The increase in temperature with a decrease in Φ_p is evident in the flat temperature region (20 mm < r < 30 mm) in Fig. 6 at z = 40 mm. The temperature increases by ~700 K as the primary air is increased. A maximum temperature of 2150 K (near-stoichiometric flame temperature) was measured at the highest primary-airflow; however, the fluctuation in temperature is only ~200 K, as compared to 400 K for the lower primary-airflow. This suggests that mixing improves with increased velocity of the air jets. The higher temperature occurs near the face of the afterbody for the higher primary-airflow and at the vortex center for the lower flow. This is thought to result from different jet mixing and residence times, local equivalence ratios, and recirculation of hot products in the cavity region as the primary-air velocity is increased.

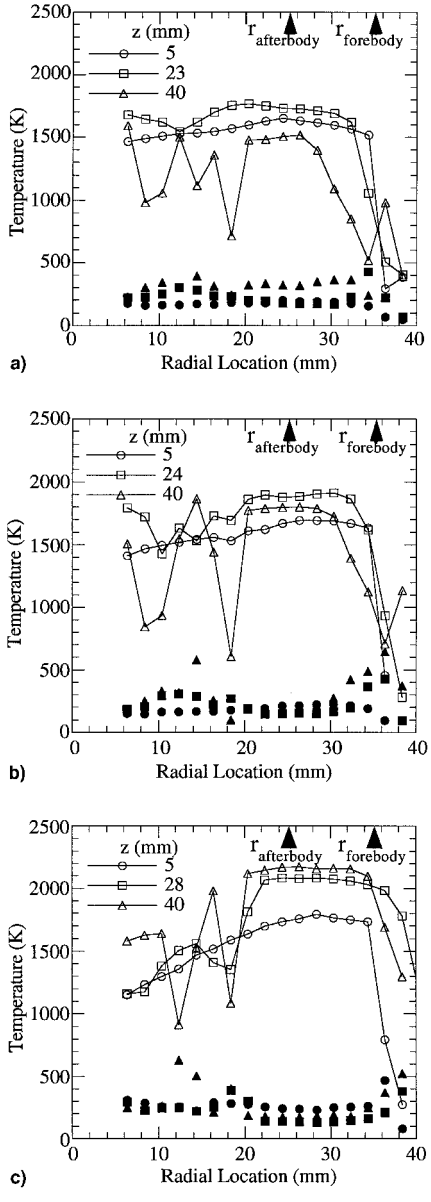

Fig. 6 Effect of primary air on temperature distributions inside cavity at U_{air} = 42 m/s and Φ_0 = 0.21. Φ_p = a) 11, b) 4.4, and c) 2.2.

Lean Blow-Out

LBO is an important design parameter for aircraft gas-turbine engines because it can impact the lower operating limits of the combustor. In gas-turbine combustors, LBO is often preceded by an unstable flame resulting from instability in the primary zone. Combustion in the primary zone then becomes intermittent, and the flame is quenched spatially and temporally. This intermittence in combustion has a direct impact on the ignition source and, as a result, the unsteadiness tends to grow until the flame blows out. In the TV combustor, the flame in the primary zone is shielded from high annular-airflow. The vortex in the cavity provides a stable ignition source through re-injection of hot products and radicals. Because the vortex is stable over a wide range of flow conditions, a TV combustor should have good LBO characteristics. The data in Fig. 3 indicate that this is the case when the primary-airflow rate is zero. The question then arises as to the influence of the primary air on the LBO limits.

The fuel and primary-airflow rates under LBO conditions are shown in Fig. 7 to illustrate the influence of primary air. The LBO experiments were conducted by fixing the primary-airflow rates and decreasing the fuel flow rate until the flame was extinguished. The LBO test was conducted with various primary-airflows and two annular-airflows. The data in Fig. 7 show that the greatest difference between the LBO for low and high annular-airflows occurs at low primary-airflows. To examine this point in more detail, it is useful to consider annular-air entrainment into the vortex when the primary air is zero.

The air involved in the LBO process must be entrained into the vortex from the annular flow when no primary air is introduced. The amount of entrainment can be estimated using LBO data in Fig. 3 for a cavity length of 0.59d_f. If one assumes that the cavity is well mixed (which is only correct to a first-order approximation), then with zero primary air, the Φ_p at LBO would correspond to the lower flammability limit of premixed propane–air flames. Through the use of Φ_p = 0.5 (lean flammability limit) and the LBO data for high annular-airflow rates in Fig. 3, it is estimated that only ~3% of the annular air is entrained into the cavity. For the low annular-airflow (U_a = 7 m/s), the estimate of entrainment is inadequate because mixing in the trapped vortex is poor. Values for air entrainment between 2.5 and 3.5% were obtained for different annular-airflow rates, which implies that the percentage of air entrained into

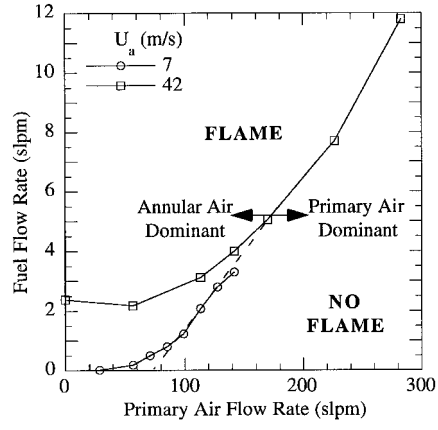

Fig. 7 Effect of primary-airflow on LBO.

the trapped vortex is relatively constant at the higher annular-airflow rates when no primary air is introduced.

As shown in Fig. 7, the fuel flow rate at LBO does not change significantly until the primary-airflow rate exceeds 60 slpm. A linear relationship between the fuel and primary-airflow rates begins to develop when primary-airflow rates are ~75 and 150 slpm for annular-air velocities of 7 and 42 m/s, respectively. At a primary-airflow rate of 175 slpm, the two curves in Fig. 7 should merge, as denoted by the dashed line. Beyond this point, the LBO depends only on the primary-airflow rate and, thus, is independent of the annular-airflow rate. The percentage of estimated air entrained into the trapped vortex increases with the primary-airflow. The assessment of entrainment using LBO data under various cavity-length and flow conditions is discussed in detail by Sturgess and Hsu.[12]

Flame Length

Flame length is important in practical combusting devices. Aircraft gas-turbine combustors are typically designed to be short to increase the thrust-to-weight ratio. State-of-the-art combustors are 15–25 cm long; therefore, the flame must be confined to this length to protect the turbine section. Advanced gas-turbine combustors operate at a maximum pressure of ~40 atm, with combustor inlet temperatures of ~1000 K. These high-pressure and -temperature conditions result in fast reaction rates and, thus, give rise to shorter flames. Typically, the flame length increases when the combustor is operated at room temperature and atmospheric pressure. Although studies of flame characteristics under ambient conditions deviate from those under practical operating conditions, such fundamental studies are often conducted in attempts to understand flame behavior as flow parameters are changed. For the present study, the flame length was examined as a function of fuel, primary air, and annular airflows.

Figure 8a shows how the visible flame length changes with fuel and annular-airflow rates at a constant primary-airflow rate of 140 slpm. The annular-airflow rates were fixed at 1000, 2000, and 3000 slpm, corresponding to annular-air velocities of 14, 28, and 42 m/s, respectively. In Fig. 8a, the data under the higher annular-airflow conditions collapsed on a single curve when the flame length was plotted as a function of the ratio of fuel to annular air (proportional to overall equivalence ratio). With a constant cavity volume and fixed primary air, the fuel is consumed at a certain rate. As the fuel flow increases, the flame length increases as a result of the excess fuel being transported and reacting in the shear layer between the cavity and annular air. A linear relationship between flame length and overall fuel-to-air ratio is observed; the slope remains constant for different annular airflows, but the y-intercept changes. An increase in annular-airflow rate with the fuel flow fixed results in a shorter flame because of enhanced turbulent mixing. However, the flame can also be quenched locally thorough vortex-flame interactions, as observed in turbulent diffusion flames. This implies that the combustion efficiency (percent of fuel consumed) decreases with increasing annular-airflow.

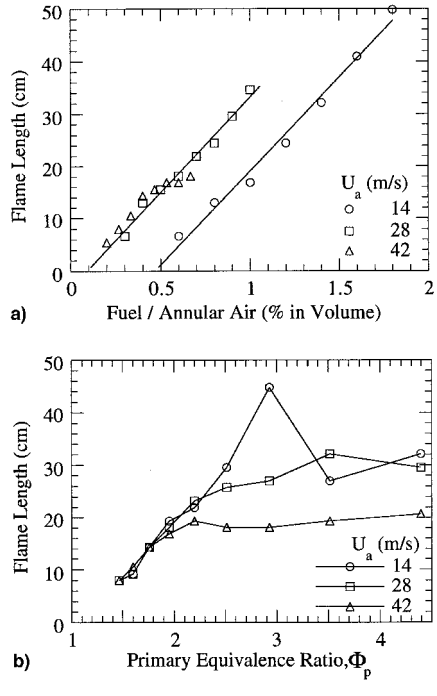

Fig. 8 Impact of flame length resulting from variations in a) fuel flow with constant primary air of 140 slpm, and b) primary equivalence ratio with constant fuel flow of 20 slpm.

Figure 8b shows the variation in flame length with Φ_p as the primary air is varied. The experiments were conducted at a fixed fuel flow rate of 20 slpm and at three fixed annular-airflow rates (1000, 2000, and 3000 slpm). In the range $\Phi_p < 2$, the flame length increased with Φ_p as the primary-airflow decreased. It is thought that the better mixing and higher temperature caused by higher primary air resulted in a shorter flame. In this flow range, the average velocity of the primary air is higher than that of the annular air. Therefore, the flame length is dominated by the primary air and is independent of the annular air, as indicated in Fig. 8b. The curves in Fig. 8b intercept at a flame length of 17 cm, which corresponds to the end of the recirculation zone established downstream of the afterbody. The wake region behind the afterbody provides another low-speed region for consumption of excess fuel. Although the length of the wake fluctuates with time, in a time-averaged view, it occurs at $2.4d_f$ downstream of the afterbody (about 17 cm from the face of the forebody).

The flame length is strongly influenced by annular-airflow in the region $\Phi_p > 2$, as shown in Fig. 8b. It is evident that the flame length remains relatively constant for a fixed annular-airflow and is reduced as the annular air is increased. In the range $\Phi_p > 2$, the primary-airflow is weak and the cavity temperature is low. The consumption of excess fuel in the annular-airstream relies mainly on mixing controlled by the annular air. Therefore, the higher annular-airflow provides better mixing, which results in a shorter flame, and the flame length remains constant at a fixed annular-airflow. Note that the shorter flame does not guarantee higher combustion efficiency, as discussed in the next section. At the lower annular-airflow (14 m/s), the flame length differs from that at higher airflows. The higher fuel-jet velocity (~17 m/s) may cause the fuel jet to become dominant.

Two-Cavity TV Combustor

The wake region behind the afterbody provides a low-speed region for further consumption of excess fuel; however, vortex shedding can cause local quenching, which can lead to reduced combustion efficiency. Little and Whipkey[7] showed that adding a second afterbody results in a significant reduction in drag. The second cavity seems to reduce the unsteady wake motion created behind the first afterbody in a one-cavity configuration. In a combusting flow, the second cavity should also improve the combustion efficiency by eliminating some of the unsteady combustion in the wake region.

Combustion Efficiency and Emissions

Figure 9 presents data on combustion efficiency and emission indices of unburned hydrocarbons (EIUHC), carbon monoxide (EICO), and oxides of nitrogen ($EINO_x$) for one-cavity (open symbols) and two-cavity (solid symbols) configurations. The test conditions were the same as those described for collection of the flame-length data in Fig. 8b. The fuel flow rate was fixed at 20 slpm (corresponding to a velocity of 17 m/s), and the annular-airflow rate was fixed at 1000, 2000, and 3000 slpm (corresponding to velocities of 14, 28, and 42 m/s, re-

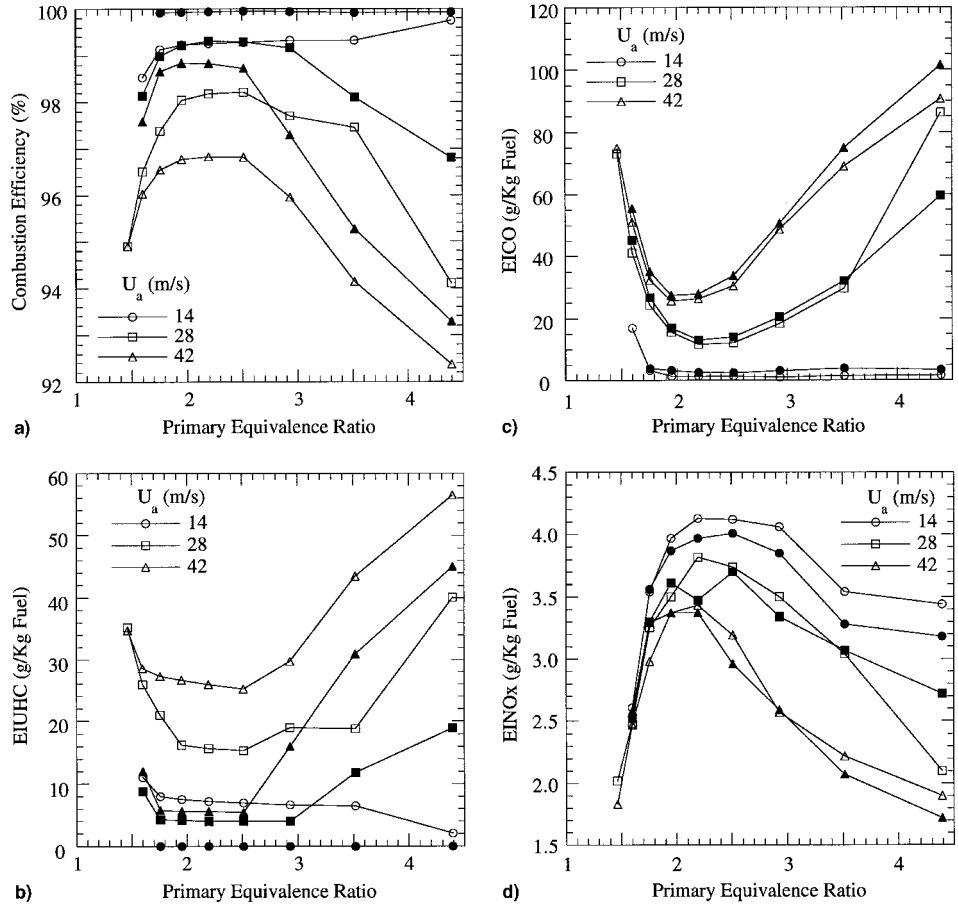

Fig. 9 Impact of primary- and annular-airflows on a) combustion efficiency and on emission indices of b) unburned hydrocarbon, c) carbon monoxide, and d) oxides of nitrogen at a fixed fuel flow. The open and solid symbols denote results from one- and two-cavity configurations, respectively.

spectively). Emissions data were collected at different primary-airflow rates. To illustrate the impact of primary air on emissions and combustion efficiency, the results are plotted as a function of Φ_p.

The characteristics of emission for the one- and two-cavity combustors showed similar trends for all of the data in Fig. 9. In general, the combustion efficiency decreases as the annular air is increased, as shown in Fig. 9a. Comparing these results and the flame-length data shown in Fig. 8b, it is clear that the shorter flame observed at high annular air is partially caused by incomplete combustion. The efficiency for the lowest annular-airflow rate is higher and flat over a wide range of Φ_p. As the annular-airflow increases, the emission and combustion efficiency become more sensitive to the primary-airflow. At the highest annular-airflow rate, the efficiency peaks at a narrower region of Φ_p between 1.8 and 2.6. A very rapid decay in efficiency takes place at low values of Φ_p (higher primary-airflow rates), and a more gradual decay occurs at higher Φ_p. It is also evident that the addition of a second afterbody (noted by the solid symbols) substantially improves the efficiency, but does not change the location of the peaks or the decay regions of the curves. Figures 9b and 9c show that inefficiency in the combustion process is the result of both UHC and CO. Even more interesting is the fact that the improvements in efficiency obtained by adding the second afterbody are mainly the result of the reduction of UHC emissions. It was also observed that CO increases slightly with the two-cavity configuration, which is a result of the additional consumption of UHC. It is also evident in comparing Figs. 9a and 9d that the NO_x and combustion efficiency peak and decay at the same values of Φ_p. The lowest NO_x and combustion efficiency occur at the highest annular-airflow rate because of the short residence time. The addition of the second cavity produces only a small difference in NO_x. Therefore, it is thought that the CO and NO_x are produced mainly in the first cavity.

Discussion

The emission characteristics are shown to be influenced by the primary- and annular-airflows when the fuel flow is maintained constant. The rapid decay that occurs in combustion efficiency, NO_x, and the flame lengths are shown in Figs. 9 and 8b for $\Phi_p < 2$. In this region, the decrease of Φ_p corresponds to increasing primary-air velocities from 40 to 52 m/s. The reduced residence times of the reacting mixture in the cavity (estimated to be 1–0.8 ms) increase the UHC and CO, as shown in Figs. 9b and 9c. The low consumption of fuel means that the heat-release rate—and, thus, the temperature in the primary zone—decreases as the primary-airflow rate increases. Both the low temperature and the reduced residence time of the reacting fuel in the primary zone are responsible for the rapid decay in combustion efficiency and NO_x in the region of $\Phi_p < 2$. Most of the NO_x is thought to be formed in the primary zone; this is supported by the temperature data in Fig. 6c. Note that temperatures are near-stoichiometric in the vicinity of the face of the first afterbody at $\Phi_p = 2.2$, which, of course, results in very high NO_x production rates. As discussed earlier, Φ_p is defined by the metered fuel and primary-airflows and does not represent the actual cavity equivalence ratio. If most of the NO_x is formed in the primary zone, then adding a second cavity should have little impact on NO_x emissions. Figure 9d shows a slight reduction of NO_x with the addition of the second cavity.

When the mixture has a short residence time in the cavity, the excess fuel will be convected downstream. Under high

primary-air conditions, a flame bulge is formed, as illustrated in Fig. 5c. The bulge extends into the annular-airstream, causing a turbulent wake to be formed downstream. The increase in turbulence in the wake region of the shear layer results in the formation of a large number of unsteady vortex structures. From the time-dependent CFD calculations reported by Katta and Roquemore,[10] unsteady flow structures are observed around the circumference of the afterbody, which causes an increase in drag. Some of the interactions in the unsteady wake regions can result in local quenching of the flame and contribute to combustion inefficiency. The intensity and frequency of the vortices generated in the shear layer and wake region increase with annular-airflow. The flow residence time also decreases as the annular air is increased. The combination of shorter fuel residence time and intensified vortex-flame interactions as the annular air is increased causes a reduction in combustion efficiency and flame length, as shown in Figs. 9a and 8b.

The improvement associated with the addition of the second cavity is an approximate measure of the combustion inefficiency resulting from the wake of the first afterbody in the one-cavity configuration. It can be noted in Fig. 9a that the improvements in combustion efficiency resulting from addition of the second cavity are greater for the higher annular-airflow rates. The frequency of vortex-flame quenching interactions, occurring in the wake and shear layer behind the first afterbody, increases with annular-air velocity. Therefore, the recirculation zone created by the second cavity significantly improves the combustion efficiency for higher annular-air conditions.

It was noted previously that the improvements in combustion efficiency resulting from the addition of the second cavity are solely a result of reductions of UHCs. In fact, the CO concentration increases slightly (see Figs. 9b and 9c). The secondary cavity provides an additional recirculation zone for fuel consumption. It is thought that the mixture is locally fuel-rich in the second cavity as a result of limited entrainment of air. Combustion in the fuel-rich second cavity favors the formation of CO rather than CO_2, as noted in Fig. 9c.

The decay in combustion efficiency at larger Φ_p is evident in Fig. 9a. The primary air directly controls the mixing and local fuel and air ratio and, as a result, influences the combustion characteristics. The entrainment and mixing of fuel into the air jets increases as the air velocity becomes much higher than the fuel velocity. On the other hand, the entrainment—and, hence, mixing—decreases as the velocity of the primary air approaches that of the fuel, as occurs for $\Phi_p > 2.6$. For example, the velocity ratios of primary air to fuel at $\Phi_p =$ 2.6 and 4.4 are 1.8 and 1.2, respectively. Under higher Φ_p conditions, the primary-zone velocity is lower than the annular-air velocity. Therefore, the excess fuel, resulting from a richer cavity, entering the shear layer is more likely to be entrained into the annular-airstream. Once the fuel is transported to the annular-air side, which is away from the ignition source, the combustion efficiency decreases as a result of increasing UHC, as shown in Figs. 9a and 9b. The increase of annular air results in higher UHC and lower efficiency. The second cavity significantly improves efficiency for the low-Φ_p condition; however, it is less effective for the high-Φ_p condition because of fuel being transported away from the wake region. The temperature in the first cavity is also related to the combustion efficiency. High reaction temperatures normally result in high efficiencies; this trend can be observed by comparing the temperatures in Figs. 6a and 6b with the combustion efficiencies in Fig. 9a for Φ_p of 4.4 and 2.2, respectively. The peak temperatures of 1800 and 2150 K correspond to efficiencies of 92 and 97%, respectively.

Conclusions

A TV concept has been investigated for flame stabilization. Fuel and primary air are injected directly into the vortex from multiple jets on the afterbody. Combustion parameters such as LBO, pressure drop, flame length, combustion efficiency, and NO_x emissions were examined for a wide range of cavity lengths and flow conditions.

It was found that the TV combustor has a low LBO limit over a wide operating range because of the cavity being shielded from the annular air. Cavity length has a strong impact on the LBO limit. A cavity length of $\sim 0.6 d_f$ was found to be optimal under various annular-airflows when no primary air is used. The primary air has a direct impact on the LBO limit as a result of mixing and residence time. The lowest LBO limits were achieved at low primary-airflow rates. At higher primary-airflows, the fuel flow rate at the LBO limit was found to increase linearly with the primary-airflow rate.

Another feature of the TV combustor is its low-pressure drop. This feature may provide significant reductions in specific fuel consumption.

Combustion efficiencies of ~99% were recorded at a low annular-air velocity of 14 m/s over a wide range of primary airflows. At a higher annular-air velocity of 42 m/s, the peak efficiency was ~97% and increased to ~99% when a second cavity was added to the combustor. Combustion is sensitive to the primary air and has a narrower high-efficiency range at higher annular-airflows. The majority of the NO_x is thought to be formed in the primary zone.

In conclusion, this paper has presented the preliminary results on the evaluation of a simple, compact, low-pressure-drop combustor utilizing the TV concept. This TV combustor exhibited good stability limits and reasonable combustion efficiencies under high-flow conditions. However, considerable work is required before the practical aspects of a TV combustor can be demonstrated. Recently, the TV concept was used for flame stabilization in developing an advanced gas-turbine combustor. In optimizing cavity performance, it was found that the combustion efficiency and LBO limits were significantly improved over a wide range of operating conditions. The aspect ratio of the cavity and the fuel and air injection scheme in the cavity have a strong impact on cavity performance. Future investigations will continue to focus on methods of improving the performance characteristics while substantially reducing NO_x. The fuel residence time and cavity entrainment that can impact practical designs will be investigated. The impact of using air to cool the cavity walls on combustion characteristics will be evaluated.

Acknowledgments

This work was supported by U.S. Air Force Contracts F33615-90-C-2033 and F33615-95-C-2507, and the Air Force Office of Scientific Research Aerospace Sciences Division. The authors would like to thank G. Sturgess and D. Burrus for helpful discussions, E. Jumper and C. Lyon for providing references and insightful discussions, and B. Sarka for assistance with the experimental work.

References

[1]Huellmantel, I. W., Ziemer, R. W., and Cambell, A. B., "Stabilization of Premixed Propane-Air Flames in Recessed Ducts," *Jet Propulsion*, Vol. 27, Jan. 1957, pp. 31–43.

[2]Morrison, C. Q., Campbell, R. L., Edelman, R. B., and Jaul, W. K., "Hydrocarbon Fueled Dual-Mode Ramjet/Scramjet Concept Evaluation," JANNAF Propulsion and Joint Subcommittee Meeting, Dec. 1996.

[3]Niioka, T., Terada, K., Hideaki, K., and Hasegawa, S., "Flame Stabilization Characteristics of Strut Divided into Two Parts in Supersonic Airflow," *Journal of Propulsion and Power*, Vol. 11, No. 1, 1995, pp. 112–116.

[4]Willis, J. W., Cadou, C., Mitchell, M., Karagozian, A. R., and Smith, O. I., "Destruction of Liquid and Gaseous Waste Surrogates in an Acoustically Excited Dump Combustor," *Combustion and Flame*, Vol. 99, No. 2, 1994, pp. 280–287.

[5]Ringleb, F. O., "Separation Control by Trapped Vortices," *Boundary Layer and Flow Control*," edited by G. V. Lachmann, Pergamon, New York, 1961, pp. 265–294.

[6]Mair, W. A., "The Effect of a Rear-Mounted Disc on the Drag of a Blunt-Based Body of Revolution," *Aeronautical Quarterly*, Vol. 10, Pt. 4, Nov. 1965, pp. 350–360.

[7]Little, B. H., Jr., and Whipkey, R. R., "Locked Vortex Afterbodies," *Journal of Aircraft*, Vol. 16, No. 5, 1979, pp. 296–302.

[8]Gharib, M., and Roshko, A., "The Effect of Flow Oscillations on Cavity Drag," *Journal of Fluid Mechanics*, Vol. 177, April 1987, pp. 501–530.

[9]Sarohia, V., and Massier, P. E., "Control of Cavity Noise," AIAA Paper 76-528, July 1976.

[10]Katta, V. R., and Roquemore, W. M., "Numerical Studies on Trapped-Vortex Concepts for Stable Combustion," *Journal of Engineering for Gas Turbines and Power* (to be published).

[11]Hsu, K.-Y., Goss, L. P., Trump, D. D., and Roquemore, W. M., "Performance of a Trapped Vortex Combustor," AIAA Paper 95-0810, Jan. 1995.

[12]Sturgess, G. J., and Hsu, K.-Y., "Entrainment of Mainstream Flow in a Trapped-Vortex Combustor," AIAA Paper 97-0261, Jan. 1997.

[13]Lefebvre, A. H., *Gas Turbine Combustion*, Taylor and Francis, Washington, DC, 1983, pp. 448–451.

[14]Goss, L. P., Post, M. E., Trump, D. D., and Sarka, B., "Two-Color Particle Imaging Velocimetry," *Journal of Laser Applications*, Vol. 3, No. 1, 1991, pp. 36–42.

[15]Post, M. E., and Goss, L. P., "Two-Color Particle-Imaging Velocimetry in Vortex Structures," AIAA Paper 93-0412, Jan. 1993.